CrossMark

Spontaneous Article

First dinosaur from the Isle of Eigg (Valtos Sandstone Formation, Middle Jurassic), Scotland

Elsa PANCIROLI[1,2]* , Gregory F. FUNSTON[2], Femke HOLWERDA[3,4,5], Susannah C. R. MAIDMENT[6], Davide FOFFA[1] , Nigel LARKIN[7], Tom CHALLANDS[2], Paige E. DEPOLO[2], Daniel GOLDBERG[2], Matthew HUMPAGE[8], Dugald ROSS[9], Mark WILKINSON[2] and Stephen L. BRUSATTE[1,2]

[1] Natural Sciences Department, National Museum of Scotland, Edinburgh EH1 1JF, Scotland, UK
[2] School of Geosciences, University of Edinburgh, Edinburgh EH9 3FE, Scotland, UK
[3] Department of Geosciences, Utrecht University, Princetonlaan 8a, 3584 CB Utrecht, the Netherlands
[4] Fachgruppe Paläoumwelt, GeoZentrum Nordbayern, Friedrich-Alexander-Universität Erlangen-Nürnberg, Loewenichstr. 28, 91054 Erlangen, Germany
[5] Royal Tyrrell Museum of Palaeontology, Drumheller, Alberta T0J 0Y0, Canada
[6] Department of Earth Sciences, Natural History Museum, Cromwell Road, London SW7 5BD, UK
[7] Cambridge University Museum of Zoology, Downing Street, Cambridge CB2 3EJ, UK
[8] Oxford, UK
[9] Staffin Museum, Ellishadder, Staffin, Isle of Skye IV51 9JE, UK
*Corresponding author. Email: elsapanciroli@googlemail.com

ABSTRACT: Dinosaur body fossil material is rare in Scotland, previously known almost exclusively from the Great Estuarine Group on the Isle of Skye. We report the first unequivocal dinosaur fossil from the Isle of Eigg, belonging to a Bathonian (Middle Jurassic) taxon of uncertain affinity. The limb bone NMS G.2020.10.1 is incomplete, but through a combination of anatomical comparison and osteohistology, we determine it most likely represents a stegosaur fibula. The overall proportions and cross-sectional geometry are similar to the fibulae of thyreophorans. Examination of the bone microstructure reveals a high degree of remodelling and randomly distributed longitudinal canals in the remaining primary cortical bone. This contrasts with the histological signal expected of theropod or sauropod limb bones, but is consistent with previous studies of thyreophorans, specifically stegosaurs. Previous dinosaur material from Skye and broadly contemporaneous sites in England belongs to this group, including *Loricatosaurus* and *Sarcolestes* and a number of indeterminate stegosaur specimens. Theropods such as *Megalosaurus* and sauropods such as *Cetiosaurus* are also known from these localities. Although we find strong evidence for a stegosaur affinity, diagnostic features are not observed on NMS G.2020.10.1, preventing us from referring it to any known genera. The presence of this large-bodied stegosaur on Eigg adds a significant new datapoint for dinosaur distribution in the Middle Jurassic of Scotland.

KEY WORDS: Bathonian, Great Estuarine Group, histology, Sauropoda, Theropoda, Thyreophora.

Dinosaurs first evolved in the Late Triassic, but remained a relatively sparse component of ecosystems until after the end-Triassic mass extinction. During the Middle Jurassic, the group underwent a significant evolutionary radiation and they became the dominant vertebrates on land for the subsequent 100 million years (Benson *et al.* 2014; Benson 2018). However, our understanding of the mode, tempo, and evolutionary drivers of this radiation are hindered by the globally sparse fossil record for dinosaurs at this time. For example, the Paleobiology Database (www.paleobiodb.org) records just 430 occurrences of Middle Jurassic dinosaurian body fossils globally. In contrast, the much better-known Late Jurassic record preserves 2100 occurrences of Dinosauria (data downloaded June 2020). This makes all contributions to the Middle Jurassic dinosaur fossil record significant.

The Inner Hebrides of Scotland yield rare Middle Jurassic dinosaur remains, but until now these have been exclusively from the Isle of Skye. The Bajocian–Bathonian Great Estuarine Group on Skye provides a vivid picture of the diverse Middle Jurassic ecosystem of the Inner Hebrides. It comprises a series of lagoonal and deltaic sedimentary rocks (Andrews 1985) that have yielded a wealth of vertebrate material, including marine, terrestrial and flying archosaurs, turtles, squamates, lissamphibians, tritylodontids, and mammaliaforms (e.g., Evans *et al.* 2006; Anquetin *et al.* 2009;

Anquetin 2010; Wills *et al.* 2014; Young *et al.* 2016a; Panciroli 2017a, b, 2018, 2019, 2020; Yi *et al.* 2017).

Dinosaur body fossils in the Great Estuarine Group remain exceptionally rare and are often fragmentary (see review in Clark 2018). From the Bathonian Valtos Sandstone Formation, they include a sauropod limb bone (Clark *et al.* 1995; Liston 2004), a sauropod tooth (Clark & Gavin 2016), two theropod teeth (Brusatte & Clark 2015; Young *et al.* 2019), and a possible basal coelurosaurian theropod caudal vertebra (Brusatte & Clark 2015). Finds from other formations within the Great Estuarine Group and underlying units include a theropod limb bone (Benton *et al.* 1995), an isolated theropod tooth (Young *et al.* 2019), isolated sauropod teeth (Barrett 2006), and a thyreophoran proximal ulna and radius (Clark 2001). Dinosaur ichnofossil tracks range from isolated tracks on loose boulders (from the Valtos Sandstone Formation, Clark & Gavin 2016, from other formations in the Great Estuarine Group, Andrews & Hudson 1984; Clark *et al.* 2005), to extensive in situ trackway sites (from the Valtos Sandstone Formation, Marshall 2005, and from other formations in the Great Estuarine Group, Clark *et al.* 2004; Marshall 2005; Brusatte *et al.* 2016; dePolo *et al.* 2018, 2020).

The Isle of Eigg has long been recognised for its fossils, particularly the 'Hugh Miller Reptile Bed', named for the prolific Victorian stonemason turned palaeontologist, geologist, and writer, Hugh Miller (1802–1856) who discovered it (Miller 1858). The reptile bed is part of the Bathonian Lealt Shale Formation (formerly 'Estheria Shales'; Hudson 1962, 1963), which underlies the Valtos Sandstone Formation (Andrews 1985; Barron *et al.* 2012). Vertebrate fossils from the Lealt Shale Formation mainly comprise isolated skeletal and dental remains of sharks, marine turtles, crocodylomorphs, and plesiosaurs (Hudson 1966; Benton 1995). A single purported dinosaur tooth from Eigg was mentioned by Rees & Underwood (2005), but this specimen was not figured and has subsequently been lost, so the identification cannot be confirmed. Despite extensive explorations of the island by Miller and contemporaries, and subsequent attention from geologists and palaeontologists in the latter half of the 20th Century (e.g., Hudson 1962, 1963, 1966; Harris & Hudson 1980; Andrews 1985), no archosaur material has been discovered in any of the other exposed sections of the Great Estuarine Group on Eigg until now.

Herein, we describe the first unequivocal Mesozoic dinosaur specimen to be found in Scotland outside of Skye. The specimen is an indeterminate limb bone – probably from a stegosaur – that was found in shoreline exposures of the Valtos Sandstone Formation on the Isle of Eigg. The specimen described here is poorly preserved, hindering higher-level taxonomic assignment, but this limitation does not negate the significance of this fossil both in the context of the Scottish dinosaur body fossil record, and for our knowledge of Middle Jurassic dinosaur palaeo-distribution.

1. Geological setting

The Great Estuarine Group (Harris & Hudson 1980; 'Great Estuarine Series' of Judd 1878, p. 722) crops out in the Scottish Inner Hebridean islands of Skye, Muck, Eigg, and Raasay (though contemporaneity of formations between the isles is by no means certain) (Fig. 1). It comprises six formations (the Cullaidh Shale Formation, Elgol Sandstone Formation, Lealt Shale Formation, Valtos Sandstone Formation, Duntulm Formation, and the Kilmaluag Formation) of Bajocian–Bathonian (Middle Jurassic) age, consisting of sedimentary rocks dominated by sandstone and mudstone, with subordinate shelly, algal, and dolomitic limestone beds (Harris & Hudson 1980; Barron *et al.* 2012). Environments represented include shallow marine,

saline, and freshwater lagoons, with tidally influenced littoral lagoons, fluvial delta lobes, and alluvial floodplains and mudflats (Barron *et al.* 2012).

The Valtos Sandstone Formation is named after the village of Valtos on the Trotternish Peninsula on the Isle of Skye, near the type section [NG 517 638 to NG 509 653] (Harris & Hudson 1980, pp. 240–243). It is underlain by the Lealt Shale Formation and overlain by the Duntulm Formation. Fossils found include: invertebrates such as the bivalve *Neomiodon* and gastropod *Viviparus*; trace fossils *Lockeia*, *Monocraterion*, *Planolites*, *Thalassinoides*, and tridactyl and ovoid footprints; coniferous wood; and fragmentary dinosaur and crocodyliform body fossils (Hudson & Harris 1979; Andrews & Hudson 1984; Clark *et al.* 1995; Barron *et al.* 2012; Brusatte & Clark 2015; Clark & Gavin 2016; Young *et al.* 2016a). The Valtos Formation represents a tidally influenced shallow littoral lagoon, frequently inundated by fluvial delta lobes, and with evidence of periodic emergence (Barron *et al.* 2012). This interpretation is supported by brackish to freshwater palynomorphs such as *Botryococcus* (Riding *et al.* 1991).

A section of the Valtos Sandstone Formation is exposed on the north-western shore of the Isle of Eigg at Camas Sgiotaig (the 'singing sands') and the bay of Laig [NM 468 905 to NM 472 885]. The limb bone NMS G.2020.10.1 was found in a loose block within Camas Sgiotaig, in a broken, but originally subspherical, calcite-cemented sandstone concretion (*sensu* Wilkinson 1992). On the Isle of Eigg, such concretions are only known from the Valtos Sandstone Formation, confirming the provenance of the specimen.

2. Materials and methods

The limb bone NMS G.2020.10.1 is part of the collection at National Museums Scotland (NMS), Edinburgh, UK. It was found by EP on a loose boulder below the high tide line south of Camas Sgiotaig on the Isle of Eigg in May 2017, during fieldwork funded by the National Geographic Society, including team members SLB, EP, TJC, PEdP, DF, and MW. It was subsequently collected under permit by SLB, DR, and DG, using a rock saw to extract the specimen. Preparation was carried out by NL: the bone was consolidated using Paraloid B72 at 5–10% in acetone, then pneumatic circular saws followed by pneumatic pens were used to remove surrounding matrix. A small <1 cm section of the bone was accidentally removed during removal of excess matrix (Fig. 2c). The natural mould of the missing mid-section of the bone was filled in with Jesmonite acrylic resin with some fibreglass matting with grey pigment.

A photogrammetric model of NMS G.2020.10.1 was created by MH using photographs taken on a Nikon D5300 and uploaded and reconstructed in Agisoft Photoscan Professional version 1.4.5. The resulting mesh was repaired and optimised in Blender 2.8.1 and then exported in .fpx format. This can be accessed freely on Sketchfab at https://sketchfab.com/3d-models/eigg-dinosaur-bone-6e670b8f91e947d6860f14016540c7bb.

A portion of the mid-shaft was removed at a natural break for osteohistological analysis by GFF, and a transverse thin section made following a modified petrographic sectioning procedure (Lamm 2013). The piece was embedded in Buehler Epothin II epoxy resin under a vacuum (−1 bar) and left to cure at room temperature for 24 h. The block was sectioned in a transverse plane using a Buehler Isomet 1000 precision saw with a table saw attachment and a diamond-tipped wafering blade. The cut billet was mounted to a polycarbonate plastic slide using Buehler Epothin II epoxy, which was left to cure at room temperature for 12 h. The mounted billet was resectioned to a thickness of 0.7 mm using a Buehler Isomet 1000 precision saw. The resectioned slide was hand-ground on a glass plate using a
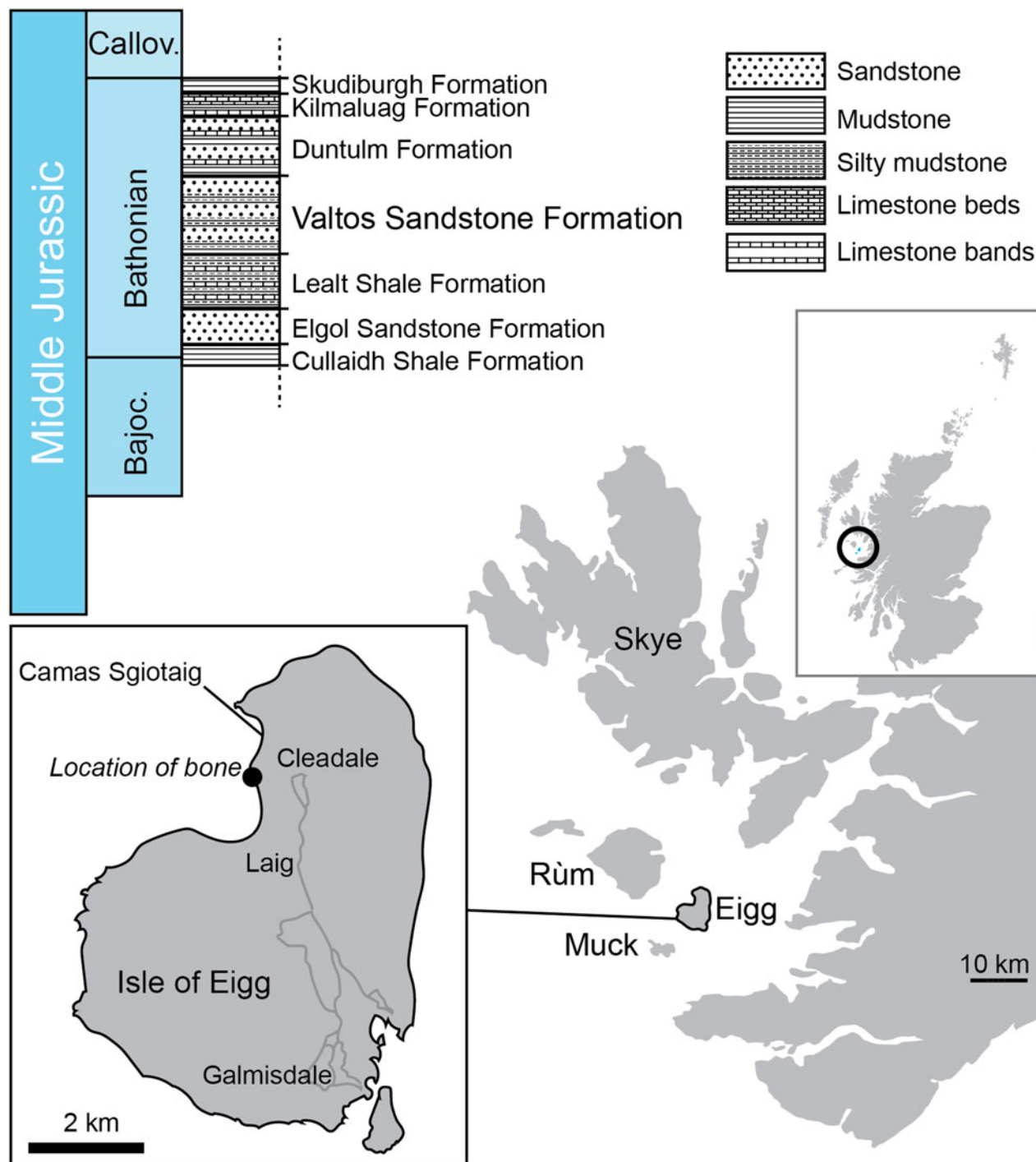
Figure 1 The lithostratigraphy of the Great Estuarine Group and location at Camas Sgiotaig on the Isle of Eigg where NMS G.2020.10.1 was found.

sequence of 220-grit, 600-grit, and 1200-grit silicon carbide abrasive powders, until the desired optical contrast was achieved. The final slide thickness was ~180 μm. The slide was polished on a short nap cloth and on a nap cloth with mineral oil to improve optical clarity.

The slide was photographed using a Nikon D7200 DSLR camera with a Nikkor 60-mm micro lens and a Nikon SB-600 Speedlight to produce transmitted light. Detailed images were taken using a Leica DMLP transmitted-light polarising microscope under normal light using Leica Application Suite 4. The polycarbonate sheet used for the slide is anisotropic, which interferes with cross-polarisation of the thin-section, so only images under normal light were taken. Images were stitched together using Adobe Photoshop 2020. Where adjustments to contrast, brightness, or colour balance were required, these modifications were applied to the entire image. Osteocyte lacunar density was calculated using the method of Cullen *et al.* (2014). Histological terminology follows Francillon-Vieillot *et al.* (1990) and Padian & Lamm (2013).

Measurements of NMS G.2020.10.1 were checked using photogrammetry models. Measurements and some figures for the comparative taxa were taken from Benson (2010), Holwerda *et al.* (in press), and Remes *et al.* (2009) in combination with the authors' (EP, FH, SCRM) own photographs of specimens.
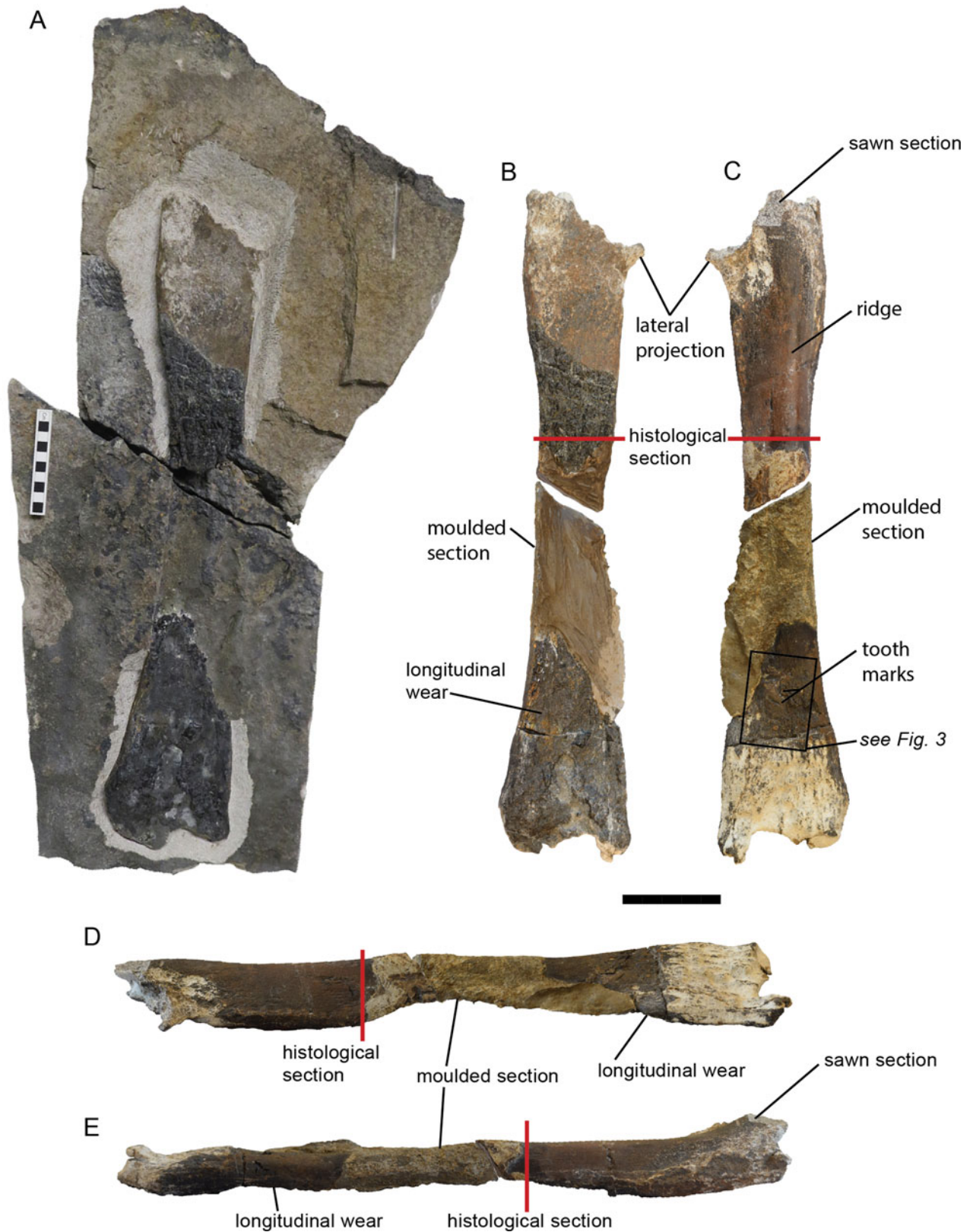
Figure 2 NMS G.2020.10.1, a probable thyreophoran limb bone from the Isle of Eigg, Scotland. (A) NMS G.2020.10.1 in matrix after initial prep. (B–E) NMS G.2020.10.1 removed from matrix and partially reconstructed: (B) the eroded 'upper' surface; (C) the surface that was downwards into the matrix; (D) and (E) side views of NMS G.2020.10.1. Scale bar = 100 mm.

Institutional abbreviations. CGP = Council for Geosciences, Pretoria, South Africa; ISIR = Indian Statistical Institute, Kolkata, India; MACN = Museo Argentino de Ciencias Naturales, Buenos Aires, Argentina; MOR = Museum of the Rockies, Montana, USA; NHMUK (previously BMNH) = Natural History Museum, London, UK; NMS = National Museums Scotland, Edinburgh, UK; OUMNH = Oxford University Museum of Natural History, Oxford, UK; PVL = Paleontologia de Vertebrados Lillo,

Universidad Nacional de Tucuman, Tucman, Argentina; QMF = Queensland Museum, Brisbane, Australia.

3. Systematic palaeontology

Superorder Dinosauria Owen, 1842
Order Ornithischia Seeley, 1887
Suborder Thyreophora Nopcsa, 1915 (*sensu* Norman, 1984)

Material. NMS G.2020.10.1, an isolated hind limb bone (Fig. 2).

Locality. Bathonian (Middle Jurassic) Valtos Sandstone Formation, Great Estuarine Group. Found on a loose boulder on the shoreline S of Camas Sgiotaig, Isle of Eigg, Scotland.

Description. NMS G.2020.10.1 is badly eroded along most of its length where exposed to weathering by the sea. It is also missing the proximal and distal ends, and is slightly compressed along its length. The total preserved length is 64 cm, and the bone is broken into two halves. Without a definitive identification, it is not possible to say which is the proximal or distal end. One half of the bone has been worn longitudinally, leaving a depth of ~5 cm of bone and exposing the internal structure (Fig. 2). The centre of the shaft is missing, but there was a natural mould of the shaft in the rock, which was used to make a reconstruction (Fig. 2) The moulded section is approximately 14 cm in length and 7.3 cm at the narrowest transverse width. There is a longitudinal ridge on the bone shaft, beginning near the break and extending to the margin of one of the broken ends (Fig. 2c), where the bone flares laterally on one side. The extent of this lateral projection is unclear because the rest of the bone is broken and missing. At least two potential tooth marks are visible on the opposite end of the bone, measuring ~2 cm in length and ~0.2 cm deep (Fig. 3a). A layer of small molluscs (probably *Neomiodon*) are present on the underside of the bone (Fig. 3b).

In the absence of the epiphyses and without a complete shaft of the bone, identification presents a challenge. Based on dimensions, comparative anatomy, and histology (see below), we suggest that NMS G.2020.10.1 is probably a stegosaur fibula.

4. Possible identity of NMS G.2020.10.1

4.1. Marine reptiles and crocodylomorphs
A variety of marine reptile (ichthyosaurs and plesiosaurs) and various crocodylomorph fossils are known from the Middle Jurassic formations of the Inner Hebrides, mostly from the Isle of Skye (Lee & Buckman 1920; Arkell 1933; Hudson 1966; Martill 1985; Clark *et al.* 1993; Benton *et al.* 1995; Brusatte *et al.* 2016; Young *et al.* 2016a; Yi *et al.* 2017). Marine reptile remains from the Isle of Eigg comprise disarticulated plesiosaurian bones from the 'Hugh Miller Bonebed' (Miller 1858; Hudson 1966).

Despite the presence of marine reptiles and crocodylomorphs in these outcrops, we do not consider NMS G.2020.10.1 to belong to any of these groups. The large size of NMS G.2020.10.1 excludes it from belonging to any of the small-bodied crocodylomorph taxa found in the Middle Jurassic of the Hebrides (e.g., Young *et al.* 2016a; Yi *et al.* 2017). Although larger-bodied thalattosuchian crocodylomorphs (teleosauroids and metriorhynchoids) have been recovered from contemporaneous Middle Jurassic formations elsewhere (Mannion *et al.* 2015; Wilberg 2015; Johnson *et al.* 2019), no thalattosuchians have yet been reported from Scotland. Even the largest thalattosuchian femora are much smaller than NMS G.2020.10.1 (e.g., ~45 cm in *Lemmysuchus obtusidens* and *Machimosaurus mosae*; Hua 1999; Young *et al.* 2016b; Johnson *et al.* 2017). The fibula/tibia is shortened compared to their femur – a modification linked to their aquatic lifestyle (Foffa *et al.* 2019). In addition, NMS G.2020.10.1 has several features that make it unlikely to belong to this clade. For example, thalattosuchian femora have a sigmoidal profile with an oval cross-section, which is not seen in NMS G.2020.10.1 (Andrews 1913; Hua & De Buffrenil 1996), although compression and poor preservation make the cross-sectional geometry difficult to assess. In large thalattosuchians, the cranial bones attained a length comparable to NMS G.2020.10.1, but the absence of articular facets, alveoli, or dermal ornamentation that characterise most thalattosuchian cranial bones (Andrews 1913) make this identification incompatible with the morphology seen here. NMS G.2020.10.1 differs histologically from crocodylomorphs in the predominance of fibrolamellar bone with abundant osteons and the absence of parallel-fibered bone in the cortex. Whereas fibrolamellar or woven bone is occasionally present in some crocodylomorphs (Woodward *et al.* 2014; Cubo *et al.* 2017), their cortices are usually formed exclusively of parallel-fibered or lamellar bone with simple vascular canals or sparse primary osteons (Hua & De Buffrénil 1996; de Andrade & Sayão 2014; Sayão *et al.* 2016; Cubo *et al.* 2017). For these reasons, we preclude this bone from being identified as that of a crocodylomorph.

The large size of NMS G.2020.10.1 also rules out attribution to an ichthyosaur or plesiosaur. Furthermore, the overall shape of NMS G.2020.10.1 does not match that of marine reptiles. The limbs of the latter are highly modified for underwater propulsion, being reduced or absent compared to terrestrial animals – as in all fully marine tetrapods (Andrews 1910). Plesiosaur and ichthyosaur limbs have short, robust humeri and femora with flared proximal and/or distal ends. The propodeal bones (radius, ulna, tibia, fibula) of these taxa are highly modified into short, often polygonal elements in the paddle (McGowan & Motani 2003; Benson 2013). The microstructure of marine reptile bones is also significantly different from that of terrestrial animals, typically showing either osteoporotic or pachyostotic textures (Hua & De Buffrenil 1996; Houssaye 2013) and does not match that found in the histological section of NMS G.2020.10.1 (see 5. Osteohistology).
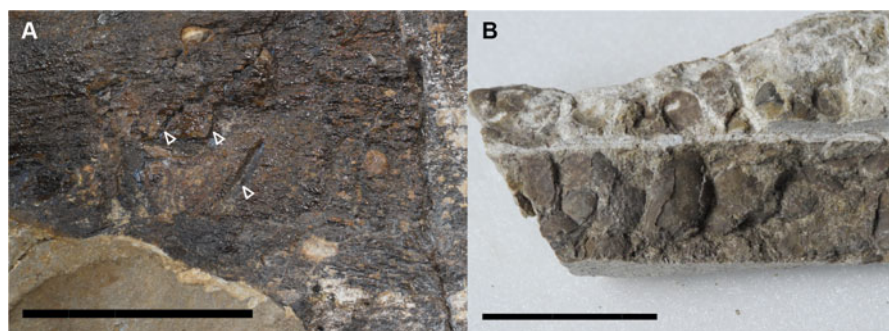

Figure 3 Possible bite marks (indicated by arrows) (A) and molluscs (B) on underside of NMS G.2020.10.1. Scale bars = 50 mm.

4.2. Theropoda

Theropod dinosaurs were the primary terrestrial carnivores during the Middle Jurassic. They ranged from those with small body masses similar to many extant birds, to medium- to large-sized genera like *Megalosaurus bucklandii* (Benson 2010), which reached body masses of ~1.4 tons (Benson *et al.* 2014) and lengths of ~8–9 m, and *Eustreptospondylus oxoniensis* (Sadlier *et al.* 2008). Both of these taxa are well-known basal tetanurans from the Middle Jurassic of England. Medium to large ceratosaurians and potentially mid-sized basal coelurosaurs (tyrannosauroids) were also present globally during this time (see review by Hendrickx *et al.* 2015).

If NMS G.2020.10.1 is a theropod dinosaur, it would belong to a mid-to-large-sized taxon. Based on size and proportions, the only theropod skeletal element NMS G.2020.10.1 could be is a femur. The length-to-width ratio is similar to the femur of Middle Jurassic *M. bucklandii* (Benson 2010, fig. 16) and *E. oxoniensis* (Sadlier *et al.* 2008, fig. 19) (Table 1; Fig. 4a–d). The lateral projection at one end of NMS G.2020.10.1 may correspond to the neck of the femoral head (with the head missing), and the opposite end may represent the distal end of a femur with the beginning of an epicondylar (flexor or extensor) groove (Fig. 4). However, the bone lacks the prominent lesser (= anterior) and fourth trochanters that characterise theropod femora. The longitudinal ridge on one half of NMS G.2020.10.1 may be the base of a lesser trochanter, but the lesser trochanters of mid-to-large-sized theropods project strongly from the anterior surface of the bone, whereas this ridge is less prominent in NMS G.2020.10.1. Even the less pronounced lesser trochanter of *Eustreptospondylus* (Fig. 3c, d) is more pronounced than in NMS G.2020.10.1. We consider it unlikely that the ridge is a damaged remnant of a more pronounced trochanter, as its surface is smooth and unbroken. It is also unlikely that a more prominent lesser trochanter was present in life but not observable because the bone has broken distal to it. If NMS G.2020.10.1 is a theropod femur, the lateral projection of the presumed proximal end indicates that only a moderate portion of the head is missing proximally. Therefore, the region that would have included the trochanter is preserved, but lacks this predominant feature. The fourth trochanter should also be visible along the posterior surface of the shaft, but appears to be absent. Although there is a large portion of the mid-shaft missing – meaning we cannot completely rule out the presence of a fourth trochanter – overall, we consider the identification of NMS G.2020.10.1 as a theropod femur unlikely.

NMS G.2020.10.1 is much larger, longer, and more slender than the humerus, radius, or ulna of *M. bucklandii* (Benson 2010, figs 12, 13) (Fig. 4e), *Eustreptospondylus* (Sadlier *et al.* 2008, fig. 16), and other mid- to large-bodied theropods, which were all bipedal animals with much shorter forelimbs than hind limbs. Although NMS G.2020.10.1 has a similar length and width as the tibia of *Megalosaurus*, NHMUK PV OR31809 (Fig. 4f, g), it lacks the twist of the shaft from proximal to distal ends observed in the tibia of *Megalosaurus*, *Eustreptospondylus* (Sadlier *et al.* 2008, fig. 20), or other theropods, and also lacks any sign of the prominent cnemial and fibular crests. NMS G.2020.10.1 also does not match the gracile and distally tapering morphology of theropod fibulae.

Histological analysis does not support the identification of NMS G.2020.10.1 as belonging to a theropod. The cancellous medullary cavity of NMS G.2020.10.1 is unlike the limb bones of most theropod dinosaurs, which are hollow. The pectoral and pelvic girdle elements of theropods have a cancellous medullary cavity, but it is difficult to reconcile the gross morphology of NMS G.2020.10.1 with these bones: theropod scapulae are flat, strap-like bones, which is not the case in NMS G.2020.10.1, and there is no evidence of a pubic apron, pubic boot, or obturator process in NMS G.2020.10.1, which eliminates a pubis or ischium as a candidate.

4.3. Sauropoda

The body fossil record for Middle Jurassic Sauropoda is relatively scarce compared to that of the Late Jurassic or Cretaceous. Material is known from China, India, North Africa, Argentina, and the UK. From the Bajocian–Bathonian of Oxfordshire and Gloucestershire, sauropods are represented by *Cetiosaurus oxoniensis* (Upchurch & Martin 2002, 2003). Finds from the NW of Scotland provide additional indeterminate sauropod material, comprising incomplete limb elements and single teeth (Clark *et al.* 1995; Liston 2004; Barrett 2006; Clark & Gavin 2016; Clark 2018).

The small size of NMS G.2020.10.1 makes it likely that if it is a sauropod limb bone, it represents a juvenile animal. The femora of contemporaneous sauropods such as *Cetiosaurus* and *Patagosaurus fariasi* are more robust than NMS G.2020.10.1, with a lower length-to-width ratio (Fig. 5a; Table 1). Cetiosaurid femora, even in juveniles, are usually anteroposteriorly flattened and mediolaterally wide, creating an elliptical cross-section (Holwerda *et al.* in press). This shape contrasts with NMS

Table 1 Measurements of NMS G.2020.10.1 and other Middle Jurassic dinosaur limb bones. Data from Benson (in press), Holwerda *et al.* (in press), Remes *et al.* (2009), and authors own photographs of specimens.

Taxon	Specimen	Bone	Length (cm)	Width (mid-shaft) (cm)	L/W ratio
Eigg dinosaur	NMS G.2020.10.1	–	64–79[1]	7.3[1]	0.11–0.09
Megalosaurus bucklandii	OUMNH J.13575	Humerus	39	6	0.15
Megalosaurus bucklandii	NHMUK PV OR36585	Ulna	23	5	0.22
Megalosaurus bucklandii	NHMUK PV OR31806	Femur	81	10	0.12
Megalosaurus bucklandii	NHMUK PV OR31809	Tibia	65	7	0.11
Cetiosaurus oxoniensis	OUMNH J.13612	Ulna	121	19	0.16
Cetiosaurus oxoniensis	OUMNH J.13615	Femur	166	30	0.18
Cetiosaurus oxoniensis	OUMNH J.29807	Fibula	57	6	0.11
Cetiosaurus oxoniensis	OUMNH J.13621	Tibia	96	17	0.18
Barapasaurus tagorei	ISIR 70	Humerus	84	12	0.14
Barapasaurus tagorei	ISIR 72	Ulna	60	7	0.12
Barapasaurus tagorei	ISIR 71	Radius	55	6	0.11
Barapasaurus tagorei	ISIR 64	Fibula	55	4	0.07
Barapasaurus tagorei	ISIR 741	Femur	93	13	0.14
Spinophorosaurus nigerensis	NMB-1698-R	Humerus	60	8	0.13
Spinophorosaurus nigerensis	GCP-CV-4229/NMB-1699-R	Femur	64	10	0.16
Spinophorosaurus nigerensis	GCP-CV-4229/NMB-1699-R	Fibula	36	4	0.11

[1]Measurements are estimated due to missing proximal and distal ends of NMS G.2020.10.1 and compression and erosion of mid-shaft, and should be considered with caution.

Figure 4 Postcranial elements of theropod dinosaurs *Megalosaurus* and *Eustreoptospondylus*. *Megalosaurus bucklandii* NHMUK PV OR31806 femur 31806 in anterior (A) and posterior (B) view; *Eustreptospondylus oxoniensis* OUMNH J.13558 femur in anterior (C) and posterior (D) view; *Megalosaurus bucklandii* OUMNH J.13575 humerus in anterior view (E); *Megalosaurus bucklandii* NHMUK PV OR31809 tibia in anterior (F) and posterior (G) view. Scale bar = 100 mm.

Figure 5 Postcranial elements of sauropod dinosaurs. *Cetiosaurus oxoniensis* femur OUMNH J.13615 in posterior view (a); *Barapasaurus tagorei* ISIR741 femur in anterior view (B) and posterior view (C); *Cetiosaurus oxoniensis* OUMNH J.29807 fibula in anterior view (D); *Rhoetosaurus brownei* QMF 1659 fibula in anterior (E) and posterior (F) view; *Spinophrosaurus nigerensis* GCP-CV-4429 fibula in anterior view (G); *Tazoudasaurus naimi* Pt-1 humerus in anterior (H) and posterior (I) view; *Cetiosaurus oxoniensis* OUMNH J.13611 ulna (J) and radius (K) in anterolateral view. Scale bar = 100 mm.

G.2020.10.1, which has a more gracile and rounded mid-shaft (Fig. 2). However, features congruent with a sauropod femur include the curved, lateral projection at one end of NMS

G.2020.10.1, which may correspond to the base of the greater trochanter, and the groove visible at the opposite end, which may represent the epicondylar groove at the distal end of the

femur (Fig. 2b, c). The femur of Early Jurassic sauropod taxon *Barapasaurus tagorei* has closer proportions to NMS G.2020.10.1 (Table 1; Fig. 5b, c), suggesting that if NMS G.2020.10.1 is a sauropod femur, it belonged to a gracile taxon, and possibly not a cetiosaurid – *Barapasaurus* is currently placed outside of the cetiosaurid clade (Holwerda & Pol 2018).

If NMS G.2020.10.1 belongs to a sauropod, we consider it most likely to be a fibula, as they are similar in length-to-width ratio to NMS G.2020.10.1 (Table 1). Sauropod fibulae bear a posterior projection on the distal end of the bone above the astragalar articular surface, as seen most clearly in *Spinophorosaurus nigeriensis* (Remes *et al*. 2009) (Fig. 5g), but also, to a lesser extent, in *C. oxoniensis* (Fig. 5d). This feature may correspond to the lateral projection at one end of NMS G.2020.10.1 (Fig. 3). Moreover, NMS G.2020.10.1 possesses a ridge which may correspond to the ridge for the accommodation of the tibia, similar to those in fibulae of the contemporaneous *Cetiosaurus* (Fig. 5d), and of the possibly Oxfordian *Rhoetosaurus brownei* (Fig. 5e, f). If that interpretation is correct, it would mean this end of NMS G.2020.10.1 corresponds to the proximal half. The somewhat triangular shape of this 'proximal' end of NMS G.2020.10.1 is similar to that in the juvenile *Cetiosaurus* OUMNH J.29807 and *Rhoetosaurus* QMF 1659.

The extreme mid-shaft compression and proximal and distal flaring of the humerus in sauropods is not present in NMS G.2020.10.1. All sauropods show this morphology, even among juvenile individuals such as *Tazoudasaurus naimi* Pt-1 (Allain & Aquesbi 2008) (Fig. 5h, i). Therefore, identification of NMS G.2020.10.1 as a sauropod humerus can be ruled out. There is no proximal flaring of the bone, as seen in the cnemial crest of sauropod tibiae. NMS G.2020.10.1 does not possess the slight sinusoidal curvature or proximal mediolateral widening and distal posterolateral widening seen in the radius of *C. oxoniensis* OUMNH J.13611 (Fig. 5k). Sauropod radii are oval in cross-section proximally (Upchurch *et al*. 2004), whereas NMS G.2020.10.1 is more triangular.

Although the length-to-width ratio is similar between NMS G.2020.10.1 and sauropod ulnae (Table 1), and there is a similar triangular cross-section near the proximal end of the bone, NMS G.2020.10.1 lacks the narrow distal end, as well as the triradiate anteromedial and anterolateral proximal expansions seen in sauropod ulnae – for example, *C. oxoniensis* OUMNH J.13611 (Fig. 5j).

4.4. Ornithischia
The Middle Jurassic body fossil record of Ornithischia is restricted to small, bipedal forms (e.g., Ruiz-Omenaca *et al*. 2006), with the exception of the armoured dinosaurs, Thyreophora, which were the first ornithischians to attain large body mass and quadrupedality (Galton & Upchurch 2004; Barrett & Maidment 2017). Thyreophoran remains are known from Middle Jurassic deposits in the UK, such as *Loricatosaurus priscus* and *Sarcolestes leedsi* from the Callovian Oxford Clay Formation (Galton 1983, 1985; Maidment *et al*. 2008), indeterminate stegosaur remains from the Sharp's Hill Formation of Oxfordshire (Boneham & Forsey 1992), and body fossils of thyreophorans from the Great Estuarine Group of the Isle of Skye (Clark 2001). There are also trackways attributed to the ichnogenus *Deltapodus* from Skye (dePolo *et al*. 2020) and the Middle Jurassic of Yorkshire (Whyte *et al*. 2007), attributed to a stegosaur trackmaker. Possible larger-bodied ornithopod footprints have recently been suggested for some of the trackways on Skye (Delair and Sarjeant, 1985, dePolo *et al*. 2020), but no conclusive evidence for their presence is currently known.

The femora of thyreophorans are proportionally short and robust, with rounded shaft cross-sections (Fig. 6a, b). In contrast, the shaft of NMS G.2020.10.1 is slender and elongate, and

flattened on one side (although this may have been accentuated by crushing). Humeri in thyreophorans are characterised by prominent deltopectoral crests that occupy much of the length of the bone, and flared distal ends (Fig. 6c, d), unlike the shape in NMS G.2020.10.1. The ulnae of thyreophorans are short, proportionally short and robust, and proximally triradiate (Fig. 6e, f), unlike NMS G.2020.10.1, and the radii are shorter and much less slender than NMS G.2020.10.1 (Fig. 6g, h). The cross-sectional geometry of NMS G.2020.10.1 is similar to the tibiae of thyreophorans (Fig. 6i, j), although the proximal and distal ends are much more flared than in NMS G.2020.10.1.

NMS G.2020.10.1 is similar in overall proportions and cross-sectional geometry to the fibulae of thyreophorans (Fig. 6i, k). It is possible, therefore, that NMS G.2020.10.1 is a fibula of a thyreophoran dinosaur. However, there are no thyreophoran synapomorphies of the fibula present (Raven & Maidment 2017) and so NMS G.2020.10.1 cannot be unequivocally referred to Thyreophora by comparative anatomy alone (but see 5. Osteohistology).

5. Osteohistology
A transverse thin section of NMS G.2020.10.1 shows it is extensively fractured and moderately crushed, which has collapsed some of the internal trabeculae (Fig. 7). Despite this damage, it is clear that the medullary cavity was not open, and that trabeculae extended throughout the medullary region. Cortical thickness is relatively high (~50%) in some regions, but varies around the cortex.

Most of the cortex is heavily remodelled, resulting in dense Haversian bone (Francillon-Vieillot *et al*. 1990), and, combined with expansion of the medullary cavity, this feature has obscured all primary bone in the inner cortex. The trabeculae of the medullary cavity are formed of lamellar bone (Francillon-Vieillot *et al*. 1990) with flattened osteocyte lacunae (Fig. 8d). Within the medullary spaces, linings of endosteally derived lamellar bone (Bromage *et al*. 2009) are apparent. The size of the medullary spaces decreases periosteally (Fig. 7b), and close to the cortex, some of the medullary spaces resemble large secondary osteons (Fig. 7a). There is a stark transition between the zone of dense Haversian bone and the trabeculae of the medullary cavity. At this transition, the diameter of vascular spaces decreases significantly and no endosteal lamellar bone is visible between the secondary osteons. The zone of dense Haversian bone is defined here as the region where secondary remodelling completely obscures any intervening primary tissue. Secondary osteons within the zone of dense Haversian bone are longitudinally oriented and decrease in size periosteally (Fig. 7a). Endosteally, several overlapping generations of secondary osteons can be discerned, and in some areas, there are at least three and maybe four generations of secondary osteons (Fig. 8c). The density of secondary remodelling decreases periosteally, so that there are fewer overlapping secondary osteons, and more primary bone is visible between them (Fig. 7d). We interpret this zone as more representative of abundant secondary remodelling rather than true dense Haversian bone, because primary tissue is visible between the secondary osteons.

In the thickest part of the cortex, an extensive area of primary bone is preserved towards the periosteal surface (Fig. 7c). This primary bone is fibrolamellar, with relatively sparse osteocyte lacunae ($\sim$14,500 mm^{-3}). Osteocyte lacunae are lenticular where they surround primary osteons, but are denser and more globose in the intermittent areas of woven bone (Fig. 8a). The primary bone is relatively poorly vascularised (Fig. 7c) compared to most dinosaurs (Horner *et al*. 1999; Horner & Padian 2004; Padian *et al*. 2004; Sander *et al*. 2011a, b; Woodward *et al*. 2015), and the density, orientation, and size of vascular canals varies throughout the cortex. In most areas, vasculature
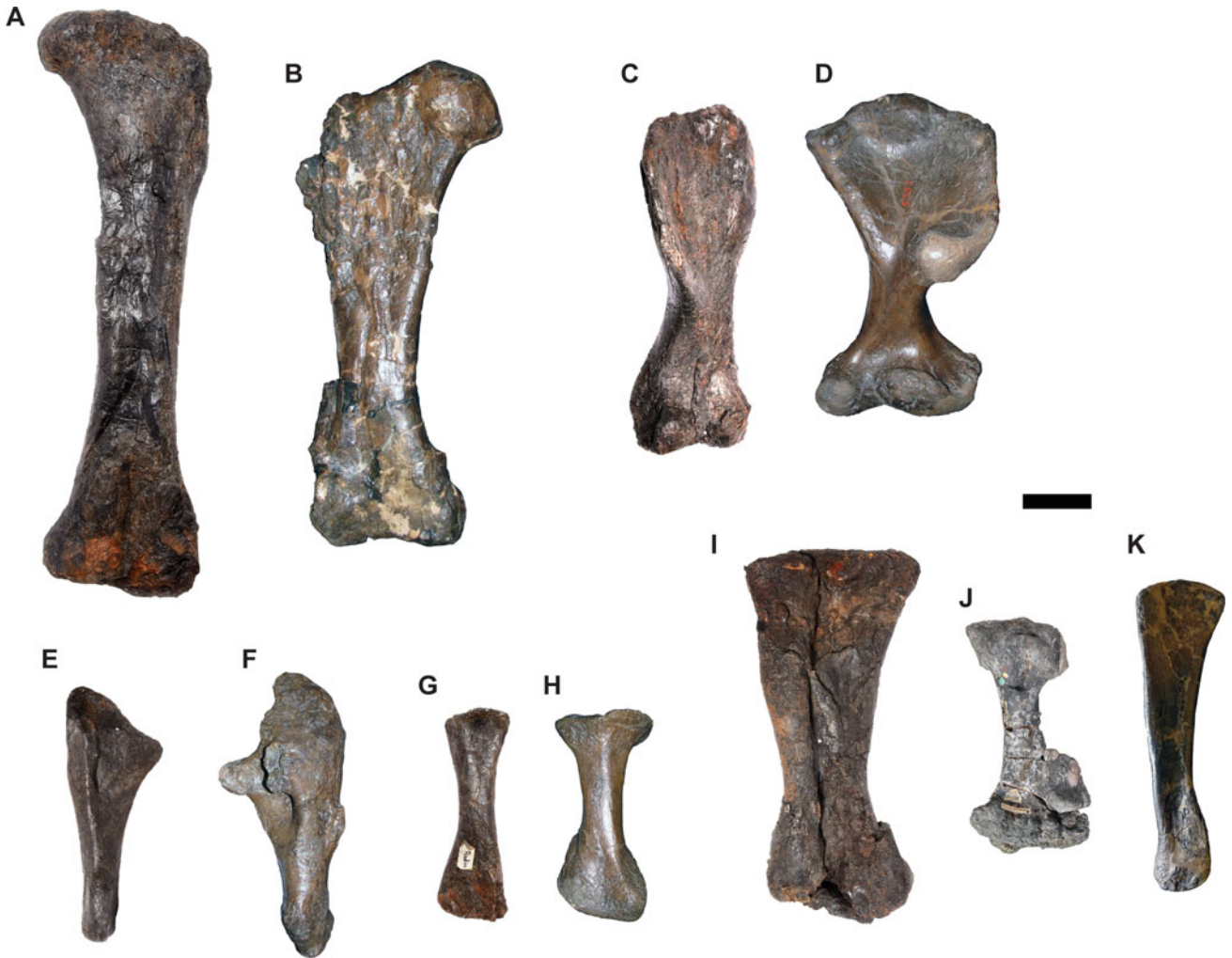
Figure 6 Postcranial elements of thyreophoran dinosaurs. Anterior views of *Stegosaurus stenops* NHMUK PV R36730 femora (A), humerus (C), ulna (E), radius (G), fused tibia and fibula (I); anterior view of *Edmontonia* sp. CMN 8531 femur (B); anterior view of *Euoplocephalus tutus* AMNH 5337 humerus (D) and radius (H); anterior view of *Euoplocephalus tutus* AMNH 5403 ulna (F); anterior view of *Polacanthus foxii* NHMUK PV R175 tibia with partial fibula fused to distal end (J); posterior view of *Ankylosaurus magniventris* AMNH 5214 fibula (K). Scale bar = 100 mm.

is longitudinal in orientation, and these canals are randomly dispersed rather than arranged into circumferential rings (Fig. 7c). Several areas have a higher proportion of anastomosing canals and thus exhibit reticular vascularity, but these are confined to small, randomly distributed patches rather than continuous layers or zones (Fig. 7c). The diameter of the longitudinal vascular canals varies randomly from ~20 μm to ~100 μm, and even adjacent canals can be considerably different in size. Vascularity is consistent in density and orientation approaching the periosteal surface, and numerous vascular canals are open to the periosteal surface (Figs 7c, d, 8f). One line of arrested growth (LAG) is visible in the primary bone of the cortex, just periosteal to the zone of Haversian bone (Fig. 7d). There are no LAGs near the periosteal surface, nor is there development of an external fundamental system (Horner *et al*. 1999; Woodward *et al*. 2011, 2015).

A region of secondary remodelling is present within the primary cortical bone, about one third of the distance from the zone of dense Haversian bone to the periosteal surface, approximately 0.5–1 mm external to the LAG (Fig. 7d). This region is separated from the Haversian bone by a band of primary fibrolamellar bone (Fig. 7d) with small, longitudinally oriented canals, where the LAG is situated (Fig. 8b). The secondary osteons in the zone of remodelling are generally larger than those in the periosteal portion of the Haversian zone, and are more comparable in size to those nearer the medullary cavity. The secondary osteons in the zone of remodelling frequently interconnect,

which creates a reticular pattern of vascularity overall (Fig. 7d). No cross-cutting of the secondary osteons can be detected, in contrast with the zone of Haversian bone. Where the primary bone is visible between the secondary osteons in this region of secondary remodelling, some erosive cavities can be discerned (Fig. 8e). These can be differentiated from primary osteons by their scalloped edges, created by Howship's lacunae, which are evidence of resorption by osteoclasts (Francillon-Vieillot *et al*. 1990).

Assuming NMS G.2020.10.1 is a hind limb bone, the bone matrix and internal structure exclude certain identifications. Fibrolamellar bone is known only in amniotes (Francillon-Vieillot *et al*. 1990), specifically in synapsids some marine reptiles (de Buffrénil & Mazin 1990; Klein 2010; Kolb *et al*. 2011; Houssaye *et al*. 2014; Klein *et al*. 2015; Wintrich *et al*. 2017), and archosaurs (Horner *et al*. 2001; de Ricqlès *et al*. 2003; Padian *et al*. 2004). The large size of the bone precludes a synapsid identification, while the lack of highly porous (osteoporotic), or compacted (pachyostotic) bone rules out marine reptiles, which have these features as adaptations for a marine lifestyle (Houssaye 2009; Houssaye *et al*. 2014). Additionally, the cortical thickness of NMS G.2020.10.1 is greater than would be expected of pelagic animals like ichthyosaurs.

The histology of NMS G.2020.10.1 is most similar to that of dinosaurs, which typically have highly vascularised fibrolamellar zonal bone with LAGs (Horner *et al*. 1999; Padian *et al*. 2004;
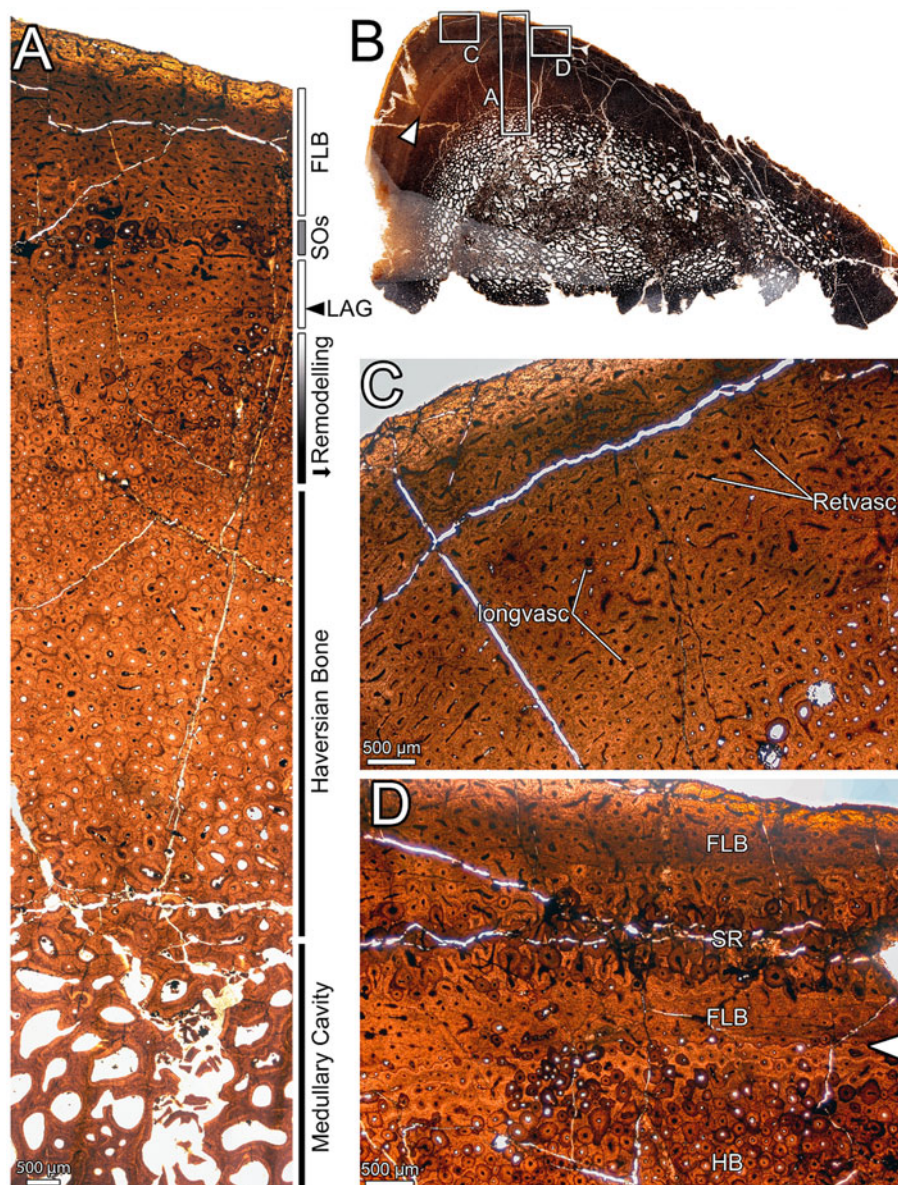
Figure 7 Overview of the osteohistology of NMS G.2020.10.1. (A) Column through the cortex, showing medullary spaces endosteally, dense Haversian bone throughout most of the cortex, and primary fibrolamellar bone in the outer cortex; (B) overview of entire slide, showing the arrangement of the medullary cavity and the cortex, and position of the LAG (arrow) in the middle cortex; (C) outer cortex, showing primary fibrolamellar bone with longitudinal–reticular vascularity and consistent vascularity to the periosteal surface; (D) outer cortex, showing zone of dense Haversian bone grading into primary fibrolamellar bone with a LAG (arrow), and a second, isolated zone of secondary remodelling. All images under normal light. Abbreviations: FLB = fibrolamellar bone; HB = Haversian bone; LAG = line of arrested growth; longvasc = longitudinal vascularity; Retvasc = reticular vascularity; SOs = secondary osteons; SR = secondary remodelling.

Padian & Lamm 2013). In contrast, crocodylomorphs and pseudosuchians more commonly show lamellar-zonal bone with lower vascularity and less fibrolamellar tissue (de Ricqlès *et al*. 2003; de Andrade & Sayão 2014; Sayão *et al*. 2016; Cubo *et al*. 2017), whereas pterosaurs have extensive medullary cavities with extremely thin cortical walls (de Ricqlès *et al*. 2000; Padian *et al*. 2004).

Detailed comparative anatomy suggests that NMS G.2020.10.1 s most likely to be either a thyreophoran or sauropod fibula. The distinctive combination of osteohistological features in NMS G.2020.10.1 provides further clues, but uncertainty over the identity of the element makes the significance of certain features – like vascular orientation – unclear. Different bones of the same individual, and even different regions within the same bone, can produce markedly different histological signatures (Horner *et al*. 1999; Cullen *et al*. 2014; Woodward *et al*. 2014; Nacarino-Meneses *et al*. 2016). Smaller bones tend to grow at

slower rates and may experience more rapid secondary remodelling (Horner *et al*. 1999), and fibulae especially tend to show more remodelling. The pervasive remodelling in NMS G.2020.10.1 may, therefore, be the result of the element rather than taxonomic identity. However, as NMS G.2020.10.1 likely represents a large hind limb bone, its histology probably generally reflects the overall growth of the individual rather than solely exhibiting a biomechanical signal.

The microstructure of NMS G.2020.10.1 differs from theropod limb bones in that the medullary cavity is not hollow (Chinsamy 1990; Horner & Padian 2004; Bybee *et al*. 2006; Lee & O'Connor 2013; Cullen *et al*. 2014). In theropods, some sparse trabeculae can be present in the medullary cavity where the diaphysis grades into the metaphysis. However, it is unlikely that the closed medullary cavity in NMS G.2020.10.1 is attributable to this phenomenon, because trabeculae completely fill the medullary cavity, and because the section was taken relatively
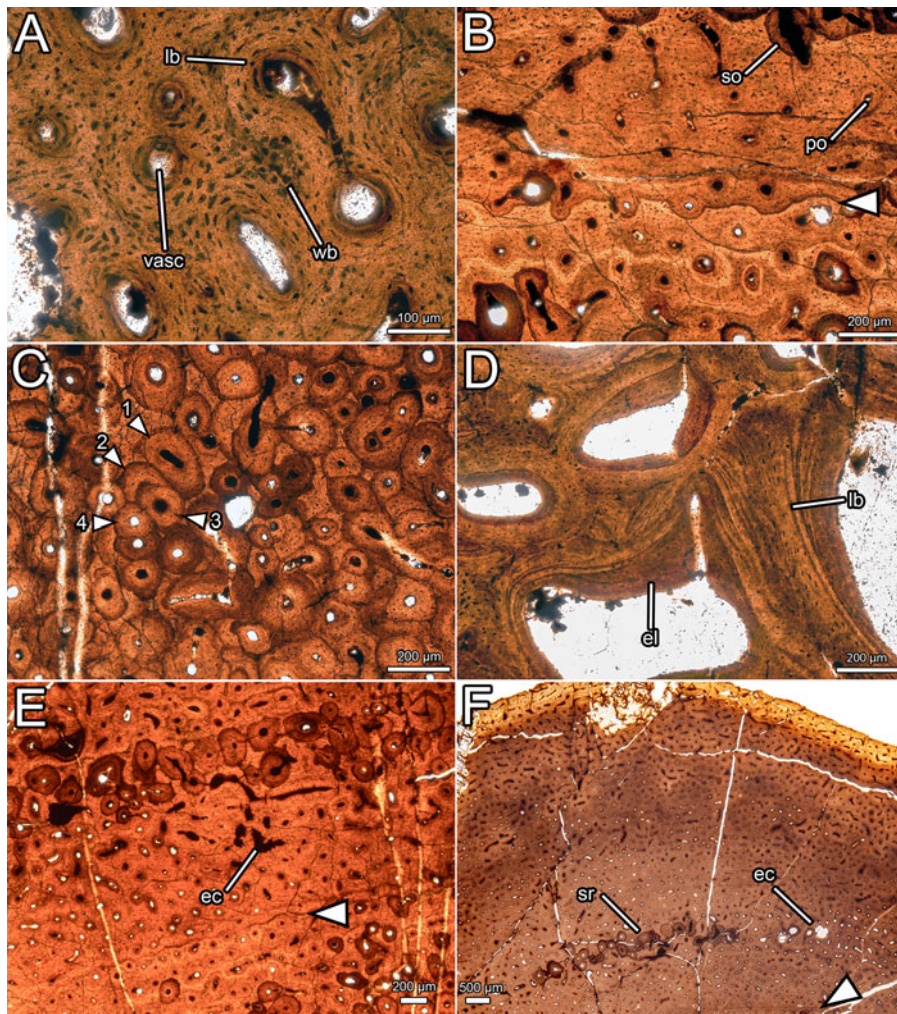
Figure 8 Histological details of NMS G.2020.10.1. (A) Primary osteons in the outer cortex, showing fibrolamellar bone matrix and variation in osteocyte shape and density; (B) primary and secondary osteons with a LAG (arrow) in the outer cortex; (C) overlapping generations of secondary osteons within the dense Haversian bone of the inner cortex (numbers indicate order of deposition); (D) trabeculae composed of lamellar bone and infilled with endosteal lamellae in the medullary cavity; (E) erosive cavities in the fibrolamellar bone separating the two zones of secondary remodelling; (F) outer cortex, showing consistent vascular orientation and density, localised secondary remodelling, and erosional cavities. All images under normal light. Abbreviations: ec = erosional cavity; el = endosteal lamellae; lb = lamellar bone; po = primary osteon; so = secondary osteon; sr = secondary remodelling; vasc = vascular canal; wb = woven bone.

close to the mid-shaft (Fig. 2). Sauropod osteohistology is well studied, and their limb bone cortices are characterised by a laminar vascular arrangement indicative of rapid growth (Sander 2000, 2004; Klein & Sander 2008; Woodward & Lehman 2009; Sander *et al.* 2011a, b), even in smaller forms (Sander *et al.* 2006; Stein *et al.* 2010). This arrangement is not the case in NMS G.2020.10.1, where vasculature is arranged randomly rather than into circumferential rows (Fig. 7c). Neosauropods tend to lack distinct LAGs (Sander *et al.* 2011a, b), and in many cases growth marks are preserved instead as polish lines visible in reflected light (de Ricqlès 1983). The presence of a LAG in NMS G.2020.10.1, therefore, argues against a neosauropod affinity for the specimen. The low osteocyte lacunar density of NMS G.2020.10.1 is further evidence against a sauropod affinity, as sauropods typically have much denser osteocyte lacunae than other comparably sized animals (Stein & Werner 2013).

Of the possible dinosaur groups, the histology of NMS G.2020.10.1 is most similar to that of thyreophoran dinosaurs. The combination of predominantly longitudinal vascularity indicative of a relatively low growth rate and abundant secondary remodelling is seen in this group (Hayashi *et al.* 2009; Redelstorff & Sander 2009; Redelstorff *et al.* 2013; Stein *et al.* 2013; Maidment *et al.* 2018). Most osteohistological work on thyreophorans has focused on their osteoderms (e.g., Hayashi *et al.* 2009; Burns

& Currie 2014; Horner *et al.* 2016), but a few studies have sampled long bones. In a review of ankylosaur osteohistology, Stein *et al.* (2013) noted abundant structural fibres within the primary and secondary bone of the limb elements of derived North American ankylosaurs. In contrast, stegosaurs lack structural fibres and have slightly less – but still abundant – secondary remodelling at equivalent ontogenetic stages (Hayashi *et al.* 2009; Redelstorff & Sander 2009; Redelstorff *et al.* 2013; Stein *et al.* 2013). Hayashi *et al.* (2009) sampled fibulae from an ontogenetic sequence of *Stegosaurus*, and Maidment *et al.* (2018) sampled a fibula of the stegosaur *Hesperosaurus*. Both showed that vasculature in medium- to large-sized individuals was predominantly longitudinal with extensive secondary remodelling and the development of LAGs.

The histology of NMS G.2020.10.1 is remarkably similar to the medium- to large-sized *Stegosaurus* fibulae described by Hayashi *et al.* (2009), except that an external fundamental system is not developed. This difference could be explained by a slightly younger ontogenetic stage in NMS G.2020.10.1, as the external fundamental system is only developed late in life (Horner *et al.* 1999; Woodward *et al.* 2011, 2015). In this aspect, NMS G.2020.10.1 is more like the fibula of *Hesperosaurus* MOR 9728 described by Maidment *et al.* (2018), which also lacks an external fundamental system. The two specimens are virtually

identical in cross-sectional shape, and although the cortical thickness of MOR 9728 is greater than NMS G.2020.10.1, this could be because the samples were taken at different locations of the mid-shaft. MOR 9728 is more extensively remodelled than NMS G.2020.10.1, but where primary bone remains near the periosteal surface, the vasculature is sparse and longitudinally oriented, as in NMS G.2020.10.1.

The osteohistological signal of slow growth with extensive remodelling is evident in *Kentrosaurus*. Based on the femora, *Kentrosaurus* had a slightly faster growth rate than *Stegosaurus* or NMS G.2020.10.1, but still lower than other comparably sized ornithischians (Redelstorff & Sander 2009; Redelstorff *et al.* 2013). NMS G.2020.10.1 shares with stegosaurs the abundant secondary remodelling (Figs 2c, 7a), randomly arranged longitudinal–reticular vasculature (Fig. 7c), and the absence of the structural fibres, as present in ankylosaurs. Of the dinosaurian candidates, the histology of NMS G.2020.10.1 is, therefore, most consistent with stegosaurs.

The fibrolamellar bone matrix of NMS G.2020.10.1 is indicative of relatively high growth rates compared to more basal tetrapods (Francillon-Vieillot *et al.* 1990; Castanet *et al.* 2000; Padian & Lamm 2013). Based on the vascular canals within the primary cortical bone, the predominantly longitudinal vascularity with small regions of reticular vascularity suggests, however, that growth in this element was on the low end of the spectrum of fibrolamellar growth rates (Castanet *et al.* 2000; de Margerie 2004). Vascularity at the periosteal surface and the absence of an external fundamental system also suggest this animal was actively growing at the time of death (Horner *et al.* 1999; Woodward *et al.* 2011, 2015).The position of the single LAG towards the middle of the cortex indicates considerable growth in the last year of life. The consistent density and orientation of vascularity in the periosteal portion of the cortex suggests that growth had not slowed, and that NMS G.2020.10.1 was in the maximum growth phase of its life when it died (Lee *et al.* 2013).

Establishing the chronological age of NMS G.2020.10.1 is difficult because of the extensive secondary remodelling of the cortex and expansion of the medullary cavity. The combination of active growth and extensive secondary remodelling is unusual, as these typically characterise different phases of growth (Klein & Sander 2008; Padian & Lamm 2013). Secondary remodelling usually progresses from the inner cortex outwards (Mitchell & Sander 2014), and, therefore, Haversian bone in the outer cortex only occurs later in life (Kerley 1965; Klein & Sander 2008). However, it can be induced by biomechanical stress or other environmental factors (Padian & Lamm 2013), which may explain the abundance of secondary osteons in conjunction with high growth rates. It is clear from the single LAG that this individual was at least one year old at the time of death, but it was almost certainly considerably older. The abundance of secondary remodelling and overlapping generations of secondary osteons are typically associated with advanced age (Kerley 1965; Uytterschaut 1993; Horner *et al.* 1999; Klein & Sander 2008; Sander *et al.* 2011a, b). Unfortunately, retrocalculation of growth marks is not possible with only a single LAG (Cooper *et al.* 2008; Lee *et al.* 2013), so the exact age of NMS G.2020.10.1 at death cannot be determined.

6. Conclusion

This specimen, NMS G.2020.10.1, is the first unequivocal dinosaur fossil found in Scotland outside of Skye. Identification of damaged isolated bones can be challenging, but finding ways to approach such identification is especially relevant for the dinosaur fossil record in Scotland, which comprises relatively incomplete material compared to contemporaneous sites in England.

Through detailed anatomical comparison, we find the overall proportions and cross-sectional geometry similar to the fibulae of thyreophorans. The length-to-width ratio and certain features such as a longitudinal ridge are similar to features present in a sauropod fibula, and NMS G.2020.10.1 bears resemblance to the fibula of juvenile *Cetiosaurus*. However, examination of the microstructure of the bone through histological analysis reveals a combination of predominantly longitudinal vascularity indicative of a relatively low growth rate, with abundant secondary remodelling – both strongly indicative of thyreophoran (particularly stegosaur) limb bone microstructure. The vascularity at the periosteal surface and absence of an external fundamental system indicate it belonged to a juvenile animal still rapidly growing at the time of death. We therefore consider NMS G.2020.10.1 most likely to represent a juvenile stegosaur fibula.

The presence of a thyreophoran bone on the Isle of Eigg adds a significant new datapoint for dinosaur distribution in the Middle Jurassic. The dinosaur body fossil record is sparse in Scotland, and this specimen provides evidence for a large-bodied animal in a locality previously not known for dinosaur fossils. Weathering, tooth marks, and a layer of small molluscs on the underside of the femur suggest transport and scavenging of the carcass prior to deposition, which is consistent with its entombment in the fluvio-deltaic Valtos Sandstone Formation.

This specimen increases the palaeontological significance of the Isle of Eigg. The island is already well known for the fossiliferous 'Hugh Miller Reptile Bed' (Miller 1858; Hudson 1966; Benton 1995), and for the distinctive features of its geological landscape, such as the Sgurr of Eigg. Although a theropod tooth fragment from Eigg was mentioned by Rees & Underwood (2005), it has subsequently been lost and this observation cannot be confirmed. This makes NMS G.2020.10.1 the first unequivocal dinosaur specimen from the island.

This discovery hints that continued exploration of the Valtos Sandstone Formation – and other parts of the Great Estuarine Group – could yield further vital fossil material. These finds would undoubtedly continue to enrich our picture of ecosystem diversity in Middle Jurassic Scotland.

7. Acknowledgements

8. References

Allain, R. & Aquesbi, N. 2008. Anatomy and phylogenetic relationships of *Tazoudasaurus naimi* (Dinosauria, Sauropoda) from the late Early Jurassic of Morocco. *Geodiversitas* **30**, 345–424.

Andrews, C. W. 1910. *A descriptive catalogue of the marine reptiles of the Oxford clay, part one.* London: British Museum (Natural History).

Andrews, C. W. 1913. *A descriptive catalogue of the marine reptiles of the Oxford clay, part two.* London: British Museum (Natural History).

Andrews, J. E. 1985. The sedimentary facies of a late Bathonian regressive episode: the Kilmaluag and Skidiburgh Formations of the Great Estuarine Group, Inner Hebrides, Scotland. *Journal of the Geological Society London* **142**, 1119–37.

Andrews, J. E. & Hudson, J. D. 1984. First Jurassic dinosaur footprint from Scotland. *Scottish Journal of Geology* **20**, 129–34.

Anquetin, J. 2010. The anatomy of the basal turtle *Eileanchelys Waldmani* from the Middle Jurassic of the Isle of Skye, Scotland. *Earth and Environmental Science Transactions of the Royal Society of Edinburgh* **101**, 67–96.

Anquetin, J., Barrett, P. M., Jones, M. E. H., Moore-Fay, S. & Evans, S. E. 2009. A new stem turtle from the Middle Jurassic of Scotland: new insights into the evolution and palaeoecology of basal turtles. *Proceedings of the Royal Society B* **276**, 879–86.

Arkell, W. J. 1933. *The Jurassic system in Great Britain*. Oxford: Oxford University Press.

Barrett, P. M. 2006. A sauropod dinosaur tooth from the Middle Jurassic of Skye, Scotland. *Transactions of the Royal Society of Edinburgh: Earth Sciences* **97**, 25–29.

Barrett, P. M. & Maidment, S. C. R. 2017. The evolution of ornithischian quadrupedality. *Journal of Iberian Earth Sciences* **43**, 463–77.

Barron, A. J. M., Lott, G. K. & Riding, J. B. 2012. Stratigraphic framework for the Middle Jurassic strata of Great Britain and the adjoining continental shelf: research report RR/11/06. British Geological Survey, Keyworth. 177 pp.

Benson, R. B. J. 2010. A description of *Megalosaurus bucklandii* (Dinosauria: Theropoda) from the Bathonian of the UK and the relationships of Middle Jurassic theropods. *Zoological Journal of the Linnean Society* **158**, 882–935.

Benson, R. B. J. 2013. Marine reptiles. *In* MacLeod, N., Archibald, J. D. & Levin, P. (eds) *Grzimek's animal life encyclopedia, extinction*, 267–79. Farmington Hills, Michigan: Gale Cengage Learning.

Benson, R. B. 2018. Dinosaur macroevolution and macroecology. *Annual Review of Ecology, Evolution, and Systematics* **49**, 379–408.

Benson, R. B. J., Campione, N. E., Carrano, M. T., Mannion, P. D., Sullivan, C., Upchurch, P. & Evans, D. C. 2014. Rates of dinosaur body mass evolution indicate 170 million years of sustained ecological innovation on the avian lineage. *PLoS Biology* **12**, e1001853.

Benton, M. J. and Spencer, P. S. 1995. British Mid Jurassic fossil reptile sites. *In* Benton, M. J. and Spencer, P. S. (eds) *Fossil Reptiles of Great Britain* 123–164. Dordrecht: Springer.

Benton, M. J., Martill, D. M. and Taylor, M. A. 1995. The first Lower Jurassic dinosaur from Scotland: limb bone of a ceratosaur theropod from Skye. *Scottish Journal of Geology* **31**, 177–182.

Boneham, B. F. W. & Forsey, G. F. 1992. Earliest stegosaur dinosaur. *Terra Nova* **4**, 628–32.

Bromage, T. G., Lacruz, R. S., Hogg, R., Goldman, H. M., McFarlin, S. C., Warshaw, J., Dirks, W., Perez-Ochoa, A., Smolyar, I., Enlow, D. H. & Boyde, A. 2009. Lamellar bone is an incremental tissue reconciling enamel rhythms, body size, and organismal life history. *Calcified Tissue International* **84**, 388–404.

Brusatte, S. L. and Clark, N. D. 2015. Theropod dinosaurs from the Middle Jurassic (Bajocian–Bathonian) of Skye, Scotland. *Geological Society of London* **51**, 157–164.

Brusatte, S. L., Challands, T. J., Ross, D. A. and Wilkinson, M. 2016. Sauropod dinosaur trackways in a Middle Jurassic lagoon on the Isle of Skye, Scotland. *Scottish Journal of Geology* **52**, 1–9.

Burns, M. E. & Currie, P. J. 2014. External and internal structure of ankylosaur (Dinosauria, Ornithischia) osteoderms and their systematic relevance. *Journal of Vertebrate Paleontology* **34**, 835–51.

Bybee, P. J., Lee, A. H. & Lamm, E.-T. 2006. Sizing the Jurassic theropod dinosaur *Allosaurus*: assessing growth strategy and evolution of ontogenetic scaling of limbs. *Journal of Morphology* **267**, 347–59.

Castanet, J., Rogers, K. C., Cubo, J. & Jacques-Boisard, J. 2000. Periosteal bone growth rates in extant ratites (ostriche and emu). implications for assessing growth in dinosaurs. *Comptes Rendus de l'Académie Des Sciences-Series III-Sciences de La Vie* **323**, 543–50.

Chinsamy, A. 1990. Physiological implications of the bone histology of *Syntarsus Rhodesiensis* (Saurischia: Theropoda). *Paleontologica Africana* **27**, 77–82.

Clark, N. D. L. 2001. A thyreophoran dinosaur from the early Bajocian (Middle Jurassic) of the Isle of Skye, Scotland. *Scottish Journal of Earth Sciences* **37**, 19–26.

Clark, N. D. L. 2018. Review of the dinosaur remains from the Middle Jurassic of Scotland, UK. *Geosciences* **8**, 53.

Clark, N. D. L., Nimmo, F. & Nicholas, C. J. 1993. A new occurrence of Scottish plesiosauran remains from the Isle of Skye. *Scottish Journal of Geology* **29**, 197–99.

Clark, N. D. L., Boyd, J. D., Dixon, R. J. & Ross, D. A. 1995. The first Middle Jurassic dinosaur from Scotland: a cetiosaurid? (Sauropoda) from the Bathonian of the Isle of Skye. *Scottish Journal of Geology* **31**, 171–76.

Clark, N. D. L., Booth, P., Booth, C. & Ross, D. A. 2004. Dinosaur footprints from the Duntulm Formation (Bathonian, Jurassic) of the Isle of Skye. *Scottish Journal of Geology* **40**, 13–21.

Clark, N. D. L., Ross, D. A. & Booth, P. 2005. Dinosaur tracks from the Kilmaluag Formation (Bathonian, Middle Jurassic) of Score Bay, Isle of Skye, Scotland, UK. *Ichnos* **12**, 93–104.

Clark, N. D. L. & Gavin, P. 2016. New Bathonian (Middle Jurassic) sauropod remains from the Valtos Sandstone Formation, Isle of Skye, Scotland. *Scottish Journal of Geology* **52**, 71–75.

Cooper, L. N., Lee, A. H., Taper, M. L. & Horner, J. R. 2008. Relative growth rates of predator and prey dinosaurs reflect effects of predation. *Proceedings of the Royal Society B: Biological Sciences* **275**, 2609–15.

Cubo, J., Köhler, M. & de Buffrénil, V. 2017. Bone histology of *Iberosuchus macrodon* (Sebecosuchia, Crocodylomorpha). *Lethaia* **50**, 495–503.

Cullen, T. M., Evans, D. C., Ryan, M. J., Currie, P. J. & Kobayashi, Y. 2014. Osteohistological variation in growth marks and osteocyte lacunar density in a theropod dinosaur (Coelurosauria: Ornithomimidae). *BMC Evolutionary Biology* **14**, 231.

de Andrade, R. C. L. P. & Sayão, J. M. 2014. Paleohistology and lifestyle inferences of a Dyrosaurid (Archosauria: Crocodylomorpha) from Paraíba Basin (Northeastern Brazil). *PLoS ONE* **9**, e102189.

de Buffrénil, V. & Mazin, J.-M. 1990. Bone histology of the ichthyosaurs: comparative data and functional interpretation. *Paleobiology* **16**, 435–47.

de Margerie, E. 2004. Assessing a relationship between bone microstructure and growth rate: a fluorescent labelling study in the king penguin chick (*Aptenodytes patagonicus*). *Journal of Experimental Biology* **207**, 869–79.

dePolo, P. E., Brusatte, S. L., Challands, T. J., Foffa, D., Ross, D. A., Wilkinson, M. & Yi, H. Y. 2018. A sauropod-dominated tracksite from Rubha nam Brathairean (Brothers' Point), Isle of Skye, Scotland. *Scottish Journal of Geology* **54**, 1–12.

dePolo, P. E., Brusatte, S. L., Challands, T. J., Foffa, D., Wilkinson, M., Clark, N. D. L., Hoad, J., da Pereira, P. V. L. G., Ross, D. A. & Wade, T. J. 2020. Novel track morphotypes from new tracksites indicate increased Middle Jurassic dinosaur diversity on the Isle of Skye, Scotland. *PLoS ONE* **15**, e0229640.

de Ricqlès, A., Padian, K., Horner, J. R. & Francillon-Vieillot, H. 2000. Palaeohistology of the bones of pterosaurs (Reptilia: Archosauria): anatomy, ontogeny, and biomechanical implications. *Zoological Journal of the Linnean Society* **129**, 349–85.

de Ricqlès, A. J. 1983. Cyclical growth in the long limb bones of a sauropod dinosaur. *Acta Palaeontologica Polonica* **28**, 225–32.

de Ricqlès, A. J., Padian, K. & Horner, J. R. 2003. On the bone histology of some Triassic pseudosuchian archosaurs and related taxa. *Annales de Paléontologie* **89**, 67–101.

Delair, J. B., and Sarjeant, W. A. S. 1985. History and bibliography of the study of vertebrate footprints in the British Isles: supplement 1973–1983. *Palaeogeography, Palaeoclimatology, Palaeoecology* **49**, 123–160.

Evans, S., Barrett, P., Hilton, J., Butler R. J., Jones, M. E. H., Liang, M.-M., Parrish, J. C., Rayfield, E. J., Sigogneau-Russell, D. & Underwood, C. J. 2006. The Middle Jurassic vertebrate assemblage of Skye, Scotland. *In* Barrett, P. & Evans, S. (eds) *Proceedings of the ninth symposium on Mesozoic terrestrial ecosystems and biota*, 36–39. London: Natural History Museum.

Foffa, D., Johnson, M. M., Young, M. T., Steel, L. & Brusatte, S. L. 2019. Revision of the Late Jurassic deep-water teleosauroid crocodylomorph *Teleosaurus Megarhinus* Hulke, 1871 and evidence of pelagic adaptations in Teleosauroidea. *PeerJ* **7**, e6646.

Francillon-Vieillot, H., de Buffrenil, V., Castanet, J., Gkraudie, J., Meunier, F. J., Sire, J. Y., Zylberberg, L. & de Ricqlès, A. J. 1990. Microstructure and mineralization of vertebrate skeletal tissues. *In* Carter J. G. (ed.) *Skeletal biomineralization: patterns, processes, and evolutionary trends*, 471–530. New York: Van Nostrand Reinhold.

Galton, P. M. 1983. *Sarcolestes leedsi* Lydekker, an ankylosaurian dinosaur from the Middle Jurassic of England. *Neues Jahrbuch für Geologie und Paläontologie Monatshefte* **3**, 141–55.

Galton, P. M. 1985. British Plated dinosaurs (Ornithischia: Stegosauria). *Journal of Vertebrate Paleontology* **11**, 211–54.

Galton, P. M. & Upchurch, P. 2004. Stegosauria. *In* Weishampel, D. B., Dodson, P. & Osmólska, H. (eds) *The Dinosauria*, 2nd edn, 343–62. Berkeley, California: University of California Press.

Harris, J. P. & Hudson, J. D. 1980. Lithostratigraphy of the Great Estuarine Group (Middle Jurassic), Inner Hebrides. *Scottish Journal of Geology* **16**, 231–50.

Hayashi, S., Carpenter, K. & Suzuki, D. 2009. Different growth patterns between the skeleton and osteoderms of *Stegosaurus* (Ornithischia: Thyreophora). *Journal of Vertebrate Paleontology* **29**, 123–31.

Hendrickx, C., Hartman, S. A. & Mateus, O. 2015. An overview of non-avian theropod discoveries and classification. *PalArch's Journal of Vertebrate Palaeontology* **12**, 1–73.

Holwerda, F. M., Rauhut, O. W. M. & Pol, D. in press. Osteological revision of the holotype of the Middle Jurassic sauropod dinosaur *Patagosaurus Fariasi* (Sauropoda: Cetiosauridae) BONAPARTE 1979. *Geodiversitas* (in press).

Holwerda, F. M. & Pol, D. 2018. Phylogenetic analysis of Gondwanan basal eusauropods from the Early-Middle Jurassic of Patagonia, Argentina. *Spanish Journal of Palaeontology* **33**, 298.

Horner, J. R., de Ricqlès, A. & Padian, K. 1999. Variation in dinosaur skeletochronology indicators: implications for age assessment and physiology. *Paleobiology* **25**, 295–304.

Horner, J. R., Padian, K. & de Ricqlès, A. 2001. Comparative osteohistology of some embryonic and perinatal archosaurs: developmental and behavioral implications for dinosaurs. *Paleobiology* **27**, 39–58.

Horner, J. R., Woodward, H. N. & Bailleul, A. M. 2016. Mineralized tissues in dinosaurs interpreted as having formed through metaplasia: A preliminary evaluation. *Comptes Rendus Palevol* **15**, 176–96.

Horner, J. R. & Padian, K. 2004. Age and growth dynamics of *Tyrannosaurus rex*. *Proceedings of the Royal Society B: Biological Sciences* **271**, 1875–80.

Houssaye, A. 2009. "Pachyostosis" in aquatic amniotes: a review. *Integrative Zoology* **4**, 325–40.

Houssaye, A. 2013. Bone histology of aquatic reptiles. *Biological Journal of the Linnean Society of London* **108**, 3–21.

Houssaye, A., Scheyer, T. M., Kolb, C., Fischer, V. & Sander, P. M. 2014. A new look at ichthyosaur long bone microanatomy and histology: implications for their adaptation to an aquatic life. *PLoS ONE* **9**, e95637.

Hua, S. 1999. Le crocodilien *Machimosaurus Mosae* (Thalattosuchia, Teleosauridae) du Kimmeridgien du Boulonnais (Pas de Calais, France). *Palaeontographica Abteilung A* **252**, 141–70.

Hua, S. & De Buffrenil, V. 1996. Bone histology as a clue in the interpretation of functional adaptations in the Thalattosuchia (Reptilia, Crocodylia). *Journal of Vertebrate Paleontology* **16**, 703–17.

Hudson, J. D. 1962. The stratigraphy of the Great Estuarine Series (Middle Jurassic) of the Inner Hebrides. *Transactions of the Edinburgh Geological Society* **19**, 139–65.

Hudson, J. D. 1963. The ecology and stratigraphical distribution of the invertebrate fauna of the Great Estuarine Series. *Palaeontology* **6**, 327–34.

Hudson, J. D. 1966. Hugh Miller's Reptile Bed and the Mytilus Shales, Middle Jurassic, Isle of Eigg, Scotland. *Scottish Journal of Geology* **2**, 265–81.

Hudson, J. D. & Harris, J. P. 1979. Sedimentology of the Great Estuarine Group (Middle Jurassic) of north-west Scotland. Symposium sur la Sédimentation de Jurassique Ouest Européen, Paris, 9–10 May 1977. Association des Sédimentologists Français, Publication Speciale Vol. 1, 1–13.

Johnson, M. M., Young, M. T. and Brusatte, S. L. 2020. Re-description of two contemporaneous mesorostrine teleosauroids (Crocodylomorpha: Thalattosuchia) from the Bathonian of England and insights into the early evolution of Machimosaurini. *Zoological Journal of the Linnean Society* **189**, 449–482.

Johnson, M. M., Young, M. T., Steel, L., Foffa, D., Smith, A. S., Hua, S., Havlik, P., Howlett, E. A. & Dyke, G. 2017. Re-description of '*Steneosaurus' obtusidens* Andrews, 1909), an unusual macrophagous teleosaurid crocodylomorph from the Middle Jurassic of England. *Zoological Journal of the Linnean Society* **1**, 1–34.

Judd, J. W. 1878. The secondary rocks of Scotland. Third paper. The strata of the western coasts and islands. *Quarterly Journal of the Geological Society of London* **34**, 660–743.

Kerley, E. R. 1965. The microscopic determination of age in human bone. *American Journal of Physical Anthropology* **23**, 149–63.

Klein, N. 2010. Long bone histology of sauropterygia from the lower Muschelkalk of the Germanic basin provides unexpected implications for phylogeny. *PLoS ONE* **5**, e11613.

Klein, N., Houssaye, A., Neenan, J. M. & Scheyer, T. M. 2015. Long bone histology and microanatomy of Placodontia (Diapsida: Sauropterygia). *Contributions to Zoology* **84**, 59–S15.

Klein, N. & Sander, M. 2008. Ontogenetic stages in the long bone histology of sauropod dinosaurs. *Paleobiology* **34**, 247–63.

Kolb, C., Sánchez-Villagra, M. R. & Scheyer, T. M. 2011. The palaeohistology of the basal ichthyosaur *Mixosaurus* (Ichthyopterygia, Mixosauridae) from the Middle Triassic: palaeobiological implications. *Comptes Rendus Palevol* **10**, 403–11.

Lamm, E.-T. 2013. Preparation and sectioning of specimens. *In* Padian, K. & Lamm, E.-T. (eds) *Bone histology of fossil Tetrapods: advancing methods, analysis, and interpretation*, 55–160. Berkeley, California: University of California Press.

Lee, A. H., Huttenlocker, A. K., Padian, K. & Woodward, H. N. 2013. Analysis of growth rates. *In* Padian, K. & Lamm, E.-T. (eds) *Bone histology of fossil Tetrapods: advancing methods, analysis, and interpretation*, 217–251. Berkeley, USA: University of California Press.

Lee, A. H. & O'Connor, P. M. 2013. Bone histology confirms determinate growth and small body size in the noasaurid theropod *Masiakasaurus knopfleri*. *Journal of Vertebrate Paleontology* **33**, 865–76.

Lee, G. W. & Buckman, S. S. 1920. *The Mesozoic Rocks of Applecross, Raasay, and North-East Skye.* Memoirs of the Geological Survey, Scotland, Edinburgh.

Liston, J. J. 2004. A re-examination of a Middle Jurassic sauropod limb bone from the Bathonian of the Isle of Skye. *Scottish Journal of Geology* **40**, 119–22.

Maidment, S. C., Norman, D. B., Barrett, P. M. and Upchurch, P. 2008. Systematics and phylogeny of Stegosauria (Dinosauria: Ornithischia). *Journal of Systematic Palaeontology* **6**, 367–407.

Maidment, S. C. R., Woodruff, D. C. & Horner, J. R. 2018. A new specimen of the ornithischian dinosaur *Hesperosaurus Mjosi* from the upper Jurassic Morrison formation of Montana, U.S.A., and implications for growth and size in Morrison stegosaurs. *Journal of Vertebrate Paleontology* **38**, e1406366.

Mannion, P. D., Benson, R. B. J., Carrano, M. T., Tennant, J. P., Judd, J. & Butler, R. J. 2015. Climate constrains the evolutionary history and bio-diversity of crocodylians. *Nature Communications* **6**, 8438.

Marshall, P. 2005. Theropod dinosaur and other footprints from the Valtos Sandstone Formation (Bathonian, Middle Jurassic) of the Isle of Skye. *Scottish Journal of Geology* **41**, 97–104.

Martill, D. M. 1985. Plesiosaur discovery in Scotland. *Geology Today* **1**, 62.

McGowan, C. & Motani, R. 2003. Ichthyopterygia. *In* Sues, H.–D. (ed), *Handbook of paleoherpetology, part 8.* Munich, Germany: Verlag Dr. Friedrich Pfeil.

Miller, H. 1858. *The cruise of the Betsey, or a summer ramble among the fossiliferous deposits of the Hebrides, and rambles of a geologist, or ten thousand miles over the fossiliferous deposits of Scotland.* Edinburgh, Scotland: NMS Publishing, Edinburgh, 2003 (facsimile of text first published 1858).

Mitchell, J. & Sander, P. M. 2014. The three-front model: a developmental explanation of long bone diaphyseal histology of Sauropoda: three-front model of long bone histology. *Biological Journal of the Linnean Society* **112**, 765–81.

Nacarino-Meneses, C., Jordana, X. & Köhler, M. 2016. Histological variability in the limb bones of the Asiatic wild ass and its significance for life history inferences. *PeerJ* **4**, e2580.

Nopcsa, F. 1915. Die Dinosaurier der siebenbürgishe Landesteile Ungarns. *Mitteilungen aus dem Jahrbüche der Königlich Ungarischen Geologischen Reichsanstalt* **23**, 1–26.

Norman, D. B. 1984. A systematic reappraisal of the reptile order Ornithischia. *In* Reif, W.-E. & Westphal, F. (eds) *Third symposium on Mesozoic terrestrial ecosystems, short papers*, 157–62. Tübingen, Germany: Attempto Verlag.

Owen, R. 1842. Report on British fossil reptiles. Part II. *Reports of the British Association for the Advancement of Science* **1841**, 60–204.

Padian, K., Horner, J. R. & De Ricqlès, A. 2004. Growth in small dinosaurs and pterosaurs: the evolution of archosaurian growth strategies. *Journal of Vertebrate Paleontology* **24**, 555–71.

Padian, K. & Lamm, E.-T. 2013. *Bone histology of fossil Tetrapods: advancing methods, analysis, and interpretation.* Berkeley, California: University of California Press.

Panciroli, E., Benson, R. B. J. & Walsh, S. 2017a. The dentary of *Wareolestes rex* (Megazostrodontidae): a new specimen from Scotland and implications for morganucodontan tooth replacement. *Papers in Palaeontology* **3**, 373–86.

Panciroli, E., Walsh, S., Fraser, N., Brusatte, S. L. & Corfe, I. 2017b. A reassessment of the postcanine dentition and systematics of the tritylodontid *Stereognathus* (Cynodontia, Tritylodontidae, Mammaliamorpha), from the Middle Jurassic of the United Kingdom. *Journal of Vertebrate Paleontology* **37**, e1351448.

Panciroli, E., Benson, R. B. J. & Butler, R. J. 2018. New partial dentaries of amphitheriid mammal *Palaeoxonodon ooliticus* from Scotland, and posterior dentary morphology in early cladotherians. *Acta Palaeontologica Polonica* **63**, 197–206.

Panciroli, E., Benson, R. B. J. & Luo, Z.-X. 2019. The mandible and dentition of *Borealestes serendipitus* (Docodonta) from the Middle Jurassic of Skye, Scotland. *Journal of Vertebrate Paleontology* **39**, e1621884.

Panciroli, E., Benson, R. B. J., Walsh, S., Butler, R. J., Castro, T. A., Jones, M. E. & Evans, S. E. 2020. Diverse vertebrate assemblage of the

Kilmaluag Formation (Bathonian, Middle Jurassic) of Skye, Scotland. *Earth and Environmental Science Transactions of The Royal Society of Edinburgh*, 1–22 [online].

Raven, T. J. & Maidment, S. C. R. 2017. A new phylogeny of Stegosauria (Dinosauria: Ornithischia). *Palaeontology* **60**, 401–08.

Redelstorff, R., Hübner, T. R., Chinsamy, A. & Sander, P. M. 2013. Bone histology of the stegosaur *Kentrosaurus aethiopicus* (Ornithischia: Thyreophora) from the Upper Jurassic of Tanzania. *The Anatomical Record* **296**, 933–52.

Redelstorff, R. & Sander, P. M. 2009. Long and girdle bone histology of *Stegosaurus*: implications for growth and life history. *Journal of Vertebrate Paleontology* **29**, 1087–99.

Rees, J. & Underwood, C. J. 2005. Hybodont sharks from the Middle Jurassic of the Inner Hebrides. *Scotland. Earth and Environmental Science Transactions of the Royal Society of Edinburgh* **96**, 351–63.

Remes, K., Ortega, F., Fierro, I., Joger, U., Kosma, R., Ferrer, J. M. M., Ide, O. A. & Maga, A. 2009. A new basal sauropod dinosaur from the Middle Jurassic of Niger and the early evolution of Sauropoda. *PLoS One* **4**, e6924.

Riding, J. B., Walton, W. & Shaw, D. 1991. Toarcian to Bathonian (Jurassic) palynology of the Inner Hebrides, Northwest Scotland. *Palynology* **15**, 115–79.

Ruiz-Omenaca, J. I., Pereda-Suberbiola, X., and Galton P. M. 2006. *Callovosaurus leedsi*, the earliest dryosaurid dinosaur (Ornithischia: Euornithopoda) from the Middle Jurassic of England. *In* Carpenter, K. (ed) *Horns and Beaks: Ceratopsian and ornithopod dinosaurs 3-16*, 3–16. Bloomington: Indiana University Press.

Sadlier, R., Barrett, P. M. & Powell, H. P. 2008. The anatomy and systematics of *Eustreptospondylus oxoniensis*, a theropod dinosaur from the Middle Jurassic of Oxfordshire, England. *Monograph of the Palaeontographical Society* **160**, 1–82.

Sander, P. 2004. Adaptive radiation in sauropod dinosaurs: bone histology indicates rapid evolution of giant body size through acceleration. *Organisms Diversity & Evolution* **4**, 165–73.

Sander, P. M. 2000. Longbone histology of the Tendaguru sauropods: implications for growth and biology. *Paleobiology* **26**, 466–88.

Sander, P. M., Mateus, O., Laven, T. & Knötschke, N. 2006. Bone histology indicates insular dwarfism in a new Late Jurassic sauropod dinosaur. *Nature* **441**, 739–41.

Sander, P. M., Klein, N., Stein, K. W. H. & Wings O. 2011a. Sauropod bone histology and its implications for sauropod biology. *In* Klein, N., Remes, K., Gee, C. & Sander, P. M. (eds) *Biology of the sauropod Dinosaurs: understanding the life of giants*, 276–304. Bloomington, Indiana: Indiana University Press.

Sander, P. M., Christian, A., Clauss, M., Fechner, R., Gee, C. T., Griebeler, E. M., Gunga, H. C., Hummel, J., Mallison, H., Perry, S. F. & Preuschoft, H. 2011b. Biology of the sauropod dinosaurs: the evolution of gigantism. *Biological Reviews* **86**, 117–55.

Sayão, J. M., Bantim, R. A. M., Andrade, R. C. L. P., Lima, F. J., Saraiva, A. A. F., Figueiredo, R. G. & Kellner, A. W. A. 2016. Paleohistology of *Susisuchus anatoceps* (Crocodylomorpha, Neosuchia): comments on growth strategies and lifestyle. *PLoS ONE* **11**, e0155297.

Seeley, H. G. 1887. On the classification of the fossil animals commonly named Dinosauria. *Proceedings of the Royal Society of London* **43**, 165–71.

Stein, K., Csiki, Z., Rogers, K. C., Weishampel, D. B., Redelstorff, R., Carballido, J. L. & Sander, P. M. 2010. Small body size and extreme cortical bone remodeling indicate phyletic dwarfism in *Magyarosaurus Dacus* (Sauropoda: Titanosauria). *Proceedings of the National Academy of Sciences* **107**, 9258–63.

Stein, K. W. H. & Werner, J. 2013. Preliminary analysis of osteocyte lacunar density in long bones of Tetrapods: all measures are bigger in sauropod Dinosaurs. *PLoS ONE* **8**, e77109.

Stein, M., Hayashi, S. & Sander, P. M. 2013. Long bone histology and growth patterns in ankylosaurs: implications for life history and evolution. *PLoS ONE* **8**, e68590.

Upchurch, P., Barrett, P. M. & Dodson, P. 2004. Sauropoda. *In* Weishampel, D. B., Dodson, P. & Osmólska, H. (eds) *The Dinosauria*, 2nd edn, 259–322. Berkeley, California: University of California Press.

Upchurch, P. & Martin, J. 2002. The Rutland *Cetiosaurus*: the anatomy and relationships of a Middle Jurassic British sauropod dinosaur. *Palaeontology* **45**, 1049–74.

Upchurch, P. & Martin, J. 2003. The anatomy and taxonomy of *Cetiosaurus* (Saurischia, Sauropoda) from the Middle Jurassic of England. *Journal of Vertebrate Paleontology* **23**, 208–31.

Uytterschaut, H. 1993. Human bone remodelling and aging. *In* Grupe, G. & Garland, A. N. (eds) *Histology of ancient human bone: methods and diagnosis*, 95–109. Berlin, Germany: Springer.

Whyte, M. A., Romano, M. and Elvidge, D. J. 2007. Reconstruction of Middle Jurassic dinosaur-dominated communities from the vertebrate ichnofauna of the Cleveland Basin of Yorkshire, UK. *Ichnos* **14**, 17–129.

Wilberg, E. W. 2015. A new metriorhynchoid (Crocodylomorpha, Thalattosuchia) from the Middle Jurassic of Oregon and the evolutionary timing of marine adaptations in thalattosuchian crocodylomorphs. *Journal of Vertebrate Paleontology* **35**, e902846.

Wilkinson, M. 1992. Concretionary cements in Jurassic sandstones, Isle of Eigg, Inner Hebrides. *Geological Society, London, Special Publications* **62**, 145–54.

Wills, S., Barrett, P. M. & Walker, A. 2014. New dinosaur and crocodylomorph from the Middle Jurassic (Bathonian) Kilmaluag Formation, Skye, Scotland. *Scottish Journal of Geology* **50**, 183–90.

Wintrich, T., Hayashi, S., Houssaye, A., Nakajima, Y. & Sander, P. M. 2017. A Triassic plesiosaurian skeleton and bone histology inform on evolution of a unique body plan. *Science Advances* **3**, e1701144.

Woodward, H. N. 2019. *Maiasaura* (Dinosauria: Hadrosauridae) tibia osteohistology reveals non-annual cortical vascular rings in young of the year. *Frontiers in Earth Science* **7**, 50.

Woodward, H. N., Horner, J. R. & Farlow, J. O. 2011. Osteohistological evidence for determinate growth in the American alligator. *Journal of Herpetology* **45**, 339–42.

Woodward, H. N., Horner, J. R. & Farlow, J. O. 2014. Quantification of intraskeletal histovariability in *Alligator mississippiensis* and implications for vertebrate osteohistology. *PeerJ* **2**, e422.

Woodward, H. N., Freedman Fowler, E. A., Farlow, J. O. & Horner, J. R. 2015. *Maiasaura*, a model organism for extinct vertebrate population biology: a large sample statistical assessment of growth dynamics and survivorship. *Paleobiology* **41**, 503–27.

Woodward, H. N. & Lehman, T. M. 2009. Bone histology and microanatomy of *Alamosaurus sanjuanensis* (Sauropoda: Titanosauria) from the maastrichtian of Big Bend National Park, Texas. *Journal of Vertebrate Paleontology* **29**, 807–21.

Yi, H., Tennant, J. P., Young, M. T., Challands, T. J., Foffa, D., Hudson, J. D., Ross, D. A. & Brusatte, S. L. 2017. An unusual small-bodied crocodyliform from the Middle Jurassic of Scotland, UK, and potential evidence for an early diversification of advanced neosuchians. *Earth and Environmental Science Transactions of the Royal Society of Edinburgh* **107**, 1–12.

Young, M. T., Tennant, J. P., Brusatte, S. L., Challands, T. J., Fraser, N. C., Clark, N. D. & Ross, D. A. 2016a. The first definitive Middle Jurassic atoposaurid (Crocodylomorpha, Neosuchia), and a discussion on the genus *Theriosuchus*. *Zoological journal of the Linnean Society* **176**, 443–62.

Young, M. T., Márton, R., Bell, M. A., Foffa, D., Steel, L., Sachs, S. & Peyer, K. 2016b. Big-headed marine crocodyliforms and why we must be cautious when using extant species as body length proxies for long-extinct relatives. *Palaeontologia Electronica* **19**, 1–14.

Young, C. M. E., Hendrickx, C., Challands, T. J., Foffa, D., Ross, D. A., Butler, I. B. & Brusatte, S. L. 2019. New theropod dinosaur teeth from the Middle Jurassic of the Isle of Skye, Scotland. *Scottish Journal of Geology* **55**, 7–19.